This article has been accepted for publication in a future issue of this journal, but has not been fully edited. Content may change prior to final publication. Citation information: DOI 10.1109/TMECH.2015.2478658, IEEE/ASME Transactions on Mechatronics

Comparison and Classification of High-precision Actuators Based on Stiffness Influencing Vibration Isolation

Shingo Ito and Georg Schitter, *Senior Member, IEEE,*

***Abstract*—Positioning performance of high-precision systems is influenced by vibrations transmitting from floors and types of the precision actuators. To construct a compact actuator with high vibration isolation for these systems, this paper investigates and categorizes precision actuators based on their stiffness for providing design rules. The effectiveness of the analysis and the design rules is confirmed by experiments comparing two types of compact precision actuators: piezoelectric and electromagnetic (Lorentz, or voice coil) actuators. The positioning system with these actuators is validated experimentally by applying step-like disturbances of approximately 160 nm to the base of the actuators. While the position error of the piezo-actuated system swings by about ± 200 nm, the Lorentz-actuated system that satisfies the design rules is able to suppress the error within a range of ± 10 nm.**

***Index Terms*—Motion control, actuators, vibrations.**

I. Introduction

MOTION control with nanometer resolution is indispensable for high-precision manufacturing machines, measurement instruments and data storage devices, such as wafer scanners [1], atomic force microscopes (AFMs) [2] and hard disk drives [3], [4]. For these systems, one of the common disturbances is vibrations transmitting from the environment. These vibrations can be reduced by using a vibration isolator as a platform [5], [6]. By selecting appropriate precision actuators, the high performance systems themselves can have high immunity against the floor vibrations, where the vibration immunity of precision actuators is related with their stiffness between the base and the moving part. They can be categorized into three groups: zero-stiffness, low-stiffness and high-stiffness actuators [7], [8].

Zero-stiffness actuators include Lorentz actuators [7], [9], where their bases (i.e. stators) and moving parts are physically decoupled by design. Since there is no mechanical connection to transmit vibrations, the moving part is not influenced by the disturbances from the base. As a result, a system with zero-stiffness actuators can achieve a position error of the nanometer level even during motion at a constant speed [1], [10]. However, in order to suspend the moving part, for example by air feet or magnetic levitation, zero-stiffness actuated systems are usually larger and heavier, limiting their achievable acceleration and positioning bandwidth [7]. (Note that Lorentz actuators consist of coils and magnets for the Lorentz force and include voice coil actuators.)

In contrast to zero-stiffness actuators, low-stiffness actuators can be compact by design to support their moving part by mechanical components with lowered stiffness [8], where typically the Lorentz force is used for the actuation [11]. While the low stiffness reduces transmitting forces due to the vibrations from the base, the residual vibrations are rejected by feedback control [8]. The control bandwidth is usually limited not by the suspension resonance, but by the internal modes of the moving part [12]. Since it can be light and rigid due to the compact design, the resonant frequencies of internal modes can be high enough. Consequently, sufficiently high control bandwidth can be achieved with feedback control for good disturbance rejection. For example, a low-stiffness system with carefully designed feedback control can position with nanometer resolution even without an additional vibration isolation [8]. These actuators are typically found in applications with low load capacity, for example optical disk drives [13], [14]. This might be to some extent because the supports with lowered stiffness have difficulties to hold a heavy mass under gravity.

High-stiffness actuators include piezoelectric actuators, which have a high intrinsic stiffness between the base and the moving part (i.e. fixed and moving end pieces) [7]. Piezo actuators can be easily miniaturized and are used for applications with extremely high control bandwidth [15], [16]. The control bandwidth of these piezo systems with feedback control is typically limited by their first or second mechanical resonance [17], [18]. Since the resonant frequency can be increased by a high stiffness of the systems, the stiffness of the piezo material itself contributes to the high resonance [19]. However, the high stiffness strongly transmits the disturbances from the base, deteriorating the positioning precision [7].

The advantages and disadvantages of each actuator category are summarized in Table I. In this actuator classification, zero-stiffness actuators are defined as ones having no mechanical stiffness between the base and the moving part [7]. In contrast, the border between low- and high-stiffness actuators is not well-defined, and thus it is unclear what stiffness is ideal to design a compact actuator with good vibration isolation capabilities. To find this border, this paper analytically investigates high-precision actuators and experimentally compares Lorentz and piezo actuated systems, resulting in a design rule to develop low-stiffness actuators that have good vibration isolation properties. In addition, the rule is related to a design

This work has been supported in part by the Austrian Research Promotion Agency (FFG) under project number 836489.

S. Ito and G. Schitter are with the Automation and Control Institute (ACIN), the Vienna University of Technology, A-1040 Vienna, Austria, e-mail: {ito, schitter}@acin.tuwien.ac.at).

This article has been accepted for publication in a future issue of this journal, but has not been fully edited. Content may change prior to final publication. Citation information: DOI 10.1109/TMECH.2015.2478658, IEEE/ASME Transactions on Mechatronics

TABLE I
CLASSIFICATION OF HIGH-PRECISION ACTUATORS

Categories	Pros	Cons
Zero-stiffness	No vibration transmission	Large and heavy
Low-stiffness	High vibration isolation	Typically for low load
High-stiffness	High control bandwidth	High vibration transmission

criteria at both the mechanical and the control design phases in the mechatronic system development.

This paper is organized as follows. Section II introduces the Lorentz and piezo actuators together with a setup for their evaluation, followed by their modeling in Section III. Section IV discusses the definition of the low- and high-stiffness actuators, as well as design requirements. Section V presents feedback control design for experimental validation in Section VI. Section VII discusses the achieved vibration isolation properties, and Section VIII concludes the paper.

II. SYSTEM DESCRIPTION

Fig. 1 shows two high-precision actuators to be compared. As the first actuator, a Lorentz actuator of a CD/DVD laser pickup (SF-HD65, Sanyo, Osaka, Japan) is selected for the high positioning performance required in a CD/DVD player and for the small size comparable with piezo actuators. Its moving part is loosely suspended by four wires, the stiffness of which is approximately 42 N/m [8]. To measure the moving part's position, an Aluminum block is placed on the objective lens as a sensor target (Fig. 1, right). The Lorentz actuator's coil has the resistance and inductance of approximately 5 Ω and 70 μH, respectively, and the voltage over the coil is proportional to the current up to about 11 kHz. Because this frequency is higher than the bandwidth of interest in the actuator comparison, a voltage amplifier is implemented to drive the Lorentz actuator, although the Lorentz force is proportional to the coil current [7].

The Lorentz actuator is compared with a ring bending piezoelectric actuator (CMBR07, Noliac, Kvistgaard, Denmark), which is capable of high-precision positioning and has a symmetrical shape with a nominal stiffness of 70 kN/m. For the position measurement, an Aluminum block is mounted on the piezo actuator (Fig. 1, left), which is driven by a high voltage amplifier (WMA-300, Falco systems, Amsterdam, Netherlands).

For the evaluation of these two actuators, a testing platform is developed as shown in Fig. 2. The platform has a fiber-optic displacement sensor (ATW-01, Unipulse, Tokyo, Japan) with a bandwidth of 100 kHz and a sensitivity of 0.341 mV/nm. This sensor is installed, such that it measures the distance to the respective Aluminum block on the actuator under testing. To generate arbitrary ground vibrations, the platform uses a shaker that moves the actuator base. The shaker consists of three 10 mm piezoelectric stack actuators (SCMAP07, Noliac, Kvistgaard, Denmark). Stack actuators in general have a high bandwidth, and thus they are suitable for generating high-frequency vibrations. The piezo stack actuators are installed without a preload to move an Aluminum plate, on which the two actuators for testing are mounted to receive common vibrations. To prevent the excitation of the rotational modes, the three stack actuators are symmetrically aligned approximately around the center of gravity of the Aluminum plate. The plate is relatively thick (10 mm) to have its internal modes at high frequencies. These stack actuators are connected electrically in parallel to a high voltage amplifier (WMA-300, Falco systems, Amsterdam, Netherlands), such that they can be actuated without exciting the undesired rotational modes of the plate.

The displacement sensor and the amplifiers are connected to a rapid prototyping control system (DS1005, dSpace GmbH, Paderborn, Germany), where feedback controllers are implemented at a sampling frequency of $f_s = 40$ kHz. Fig. 3 shows a block diagram of the overall setup. One of the inputs to the system is the amplifier reference for the shaker u_b to generate vibrations x_b at the actuator base as disturbances. The other input is the amplifier reference for the actuator under testing u_a to generate the actuator force F for regulating the actuator position x_m with nanometer resolution by feedback control. The signal y is the output voltage of the sensor with sensitivity K_s. The transfer function $P_a(s)$ and $P_t(s)$ represent the dynamics of the mechanical system, and $G(s)$ is for the dynamics due to the electronics and the electrical system.

For calibration and analysis of the shaker, the frequency response of the shaker is determined. For this analysis, the sensor position is temporary adjusted to measure x_b, and a Bode plot is measured from u_b to x_b. Since the piezoelectric stack actuators of the shaker are mounted without a preload, the frequency of the sine sweep is limited to 2 kHz to avoid pulling forces that may damage the actuators. Fig. 4 shows a Bode plot measured by a network analyzer (3562A, Hewlett Packard, Palo Alto, USA). From the flat gain below 100 Hz, the sensitivity of the shaker is calculated as 1621 nm/V, which is used to correct measured data as calibration in Section VI. Above 100Hz, the shaker has parasitic dynamics. This dynamics is not mathematically modeled as the shaker is only used to generate the same disturbances for both actuators, which can be regarded as a coloring of the noise as it may happen under real conditions.

The respective frequency responses of the bending piezo and Lorentz actuators are also measured by the network analyzer. Fig. 5 shows the measured Bode plot from u_a to y for both actuators. The blue solid line is the response of the bending piezo, and its first resonance can be seen at a relatively high frequency of approximately 990 Hz. In contrast, the Lorentz actuator's response, represented by the red dashed line, shows its first resonance at a low frequency of 54 Hz. In both cases, the actuators do not obviously excite the parasitic dynamics of the shaker (e.g. the resonance at 500 Hz as seen in Fig. 4). This is because the actuator base including the 10 mm Aluminum plate is much heavier than the moving part, and the base movement resulting from the actuator's counterforce can be ignored. The black dash-dot lines in Fig. 5 represent the fitted models to be discussed in the next section.

Post-print version of the article: S. Ito and G. Schitter, "Comparison and Classification of High-Precision Actuators Based on Stiffness Influencing Vibration Isolation," *IEEE/ASME Transactions on Mechatronics*, vol. 21(2), pp. 1169-1178, 2016. DOI: 10.1109/TMECH.2015.2478658

This article has been accepted for publication in a future issue of this journal, but has not been fully edited. Content may change prior to final publication. Citation information: DOI 10.1109/TMECH.2015.2478658, IEEE/ASME Transactions on Mechatronics

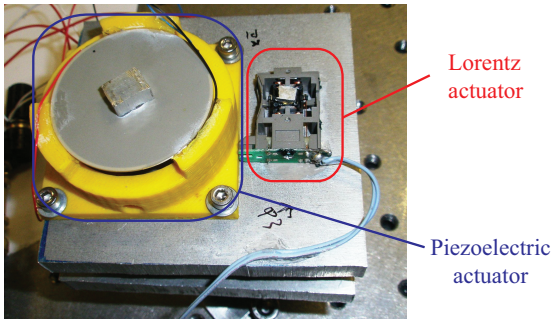

Fig. 1. High-precision actuators for comparison: Ring bending piezoelectric actuator (left) and Lorentz actuator of a laser pickup (right).

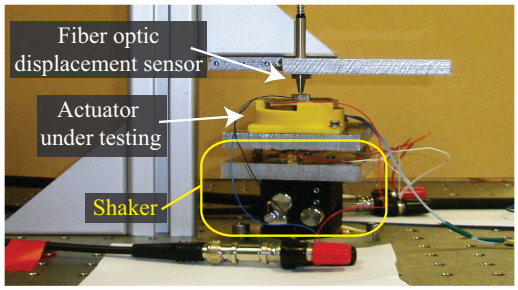

Fig. 2. Photograph of testing platform. The position of an actuator under testing is measured by a displacement sensor on a shaker.

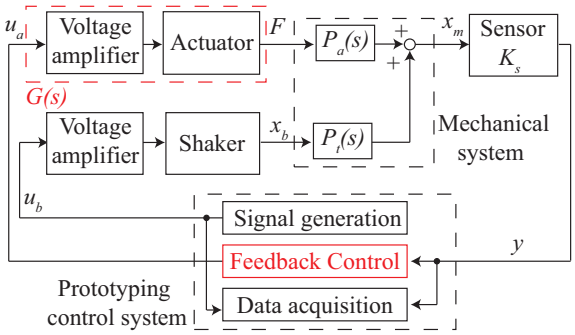

Fig. 3. Block diagram of experimental setup. While the shaker with the input u_b is used to generate vibrations x_b, the position of an actuator under testing x_m is controlled with nanometer resolution by the feedback control. The reference of the actuator amplifier is u_a, and F is the actuator force. The signal y is the output voltage of the sensor with sensitivity of K_s. Transfer function $P_a(s)$ and $P_t(s)$ represent the mechanical dynamics, and $G(s)$ is for the dynamics due to the electronics and the electric system.

III. Modeling

For discussion on the actuator categories and design rules in Section IV, as well as control design in Section V, an actuator model is derived in this section.

A. Dynamics of mechanical system

The high-precision actuators presented in the previous section can be modeled as shown in Fig. 6, where m, k and c are

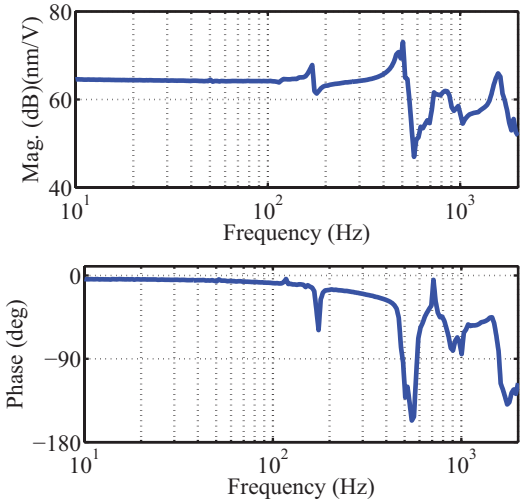

Fig. 4. Bode plot of shaker from amplifier reference u_b to position x_b. The position is measured by the fiber-optic sensor while the three piezoelectric stack actuators are moving.

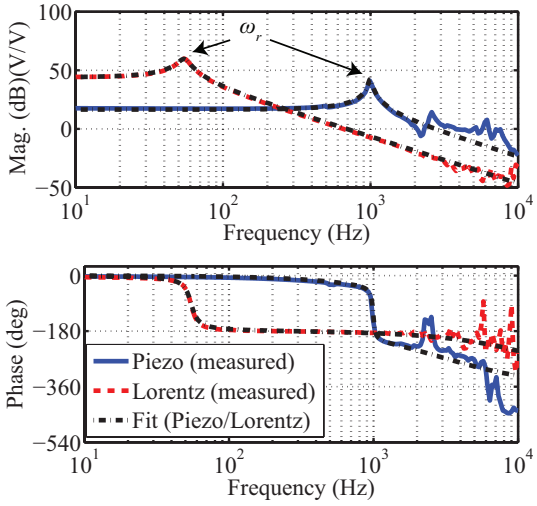

Fig. 5. Bode plot of bending piezo and Lorentz actuators measured from amplifier reference u_a to sensor output y, as well as their models. The arrows indicate the actuators' first resonant frequency ω_r.

the mass, the spring constant and the damping coefficient of the actuators, respectively. From the lumped-mass model, an equation of motion is given as follows

$$m\ddot{x}_m + c(\dot{x}_m - \dot{x}_b) + k(x_m - x_b) = F, \qquad (1)$$

where F is the actuator force, x_b represents ground vibrations, and x_m is the moving part's position to be controlled with nanometer resolution. After the Laplace transformation of the above equation and re-arranging it, the actuator position can be shown in the following form

$$X_m(s) = P_a(s)F(s) + P_t(s)X_b(s), \qquad (2)$$

Post-print version of the article: S. Ito and G. Schitter, "Comparison and Classification of High-Precision Actuators Based on Stiffness Influencing Vibration Isolation," *IEEE/ASME Transactions on Mechatronics*, vol. 21(2), pp. 1169-1178, 2016. DOI: 10.1109/TMECH.2015.2478658

This article has been accepted for publication in a future issue of this journal, but has not been fully edited. Content may change prior to final publication. Citation information: DOI 10.1109/TMECH.2015.2478658, IEEE/ASME Transactions on Mechatronics

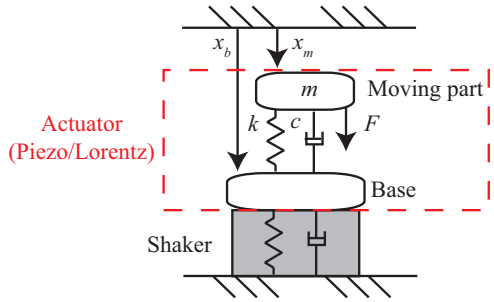

Fig. 6. Lumped mass model of precision actuator on testing platform.

using

$$P_a(s) = \frac{X_m(s)}{F(s)} = \frac{1}{ms^2 + cs + k}, \tag{3}$$

$$P_t(s) = \frac{X_m(s)}{X_b(s)} = \frac{cs + k}{ms^2 + cs + k}, \tag{4}$$

where $X_m(s)$, $X_b(s)$ and $F(s)$ are the Laplace transformation of x_m, x_b and F, respectively. The transfer function $P_t(s)$ is from the actuator base to the moving part position and is the transmissibility of the system [7].

B. Dynamics of electronics and electrical system

The derived mechanical model (3) is a minimum phase system and does not model any delay. Nevertheless, the measured Bode plot in Fig. 5 shows a delay of approximately 20 μs for the Lorentz and 100 μs for the piezo actuator. Since the delay is different for each actuator despite the use of the same sensor, it can be assumed that the actuator amplifiers cause the majority of this delay. In order to capture it, the transfer function to relate the amplifier reference u_a with the actuator force F is given by using the first-order Pade approximation [3]

$$G(s) = \frac{F(s)}{U_a(s)} = \frac{1 - \frac{\tau}{2}s}{1 + \frac{\tau}{2}s} K_a K_f, \tag{5}$$

where $U_a(s)$ is the Laplace transformation of u_a and τ is the delay, as well as the gain of the respective amplifier K_a. The constant K_f is the force-to-voltage ratio of the respective actuator. For the bending piezo, it is approximated by the ratio of the blocking force and the maximum operational voltage, while for the Lorentz actuator it is by the ratio of the motor constant and the coil resistance.

Nonlinearity of piezos (e.g. hysteresis or creep) [7] can be a problem when they are used in an open-loop control or when their control input is utilized (e.g. AFMs). However, when these actuators are used in a closed loop with a position sensor, such nonlinearity is typically well-compensated by the feedback controller (cf. [20]). Since the actuators in this paper are compared in a closed loop for vibration isolation, the nonlinearity is not modeled.

The fiber-optic displacement sensor has a bandwidth of 100 kHz, which is 10 times higher than the frequency band of

TABLE II
ESTIMATED PARAMETERS OF ACTUATOR MODEL

Parameters	Piezo	Lorentz
g	6.68	158
ζ	0.025	0.083
ω_n	$2\pi\cdot 995$	$2\pi\cdot 54.7$
τ	100 μs	20 μs

Fig. 5. Even if the sensor may cause a phase lag, it is incorporated into (5). Therefore, the sensor dynamics is treated as a constant, which is the sensor sensitivity K_s = 0.341 mV/nm.

C. Parameter estimation

Using the introduced models (3) and (5), the transfer function from u_a to y is given as $G(s)P_a(s)K_s$ and can be re-arranged as follows

$$G(s)P_a(s)K_s = \left(\frac{g}{\frac{s^2}{\omega_n^2} + 2\zeta\frac{s}{\omega_n} + 1}\right)\left(\frac{1 - \frac{\tau}{2}s}{1 + \frac{\tau}{2}s}\right), \tag{6}$$

where g is the gain, ζ is the damping ratio, and ω_n is the undamped natural frequency [7] given as

$$g = \frac{K_s K_a K_f}{k}, \qquad \zeta = \frac{c}{2\sqrt{km}}, \qquad \omega_n = \sqrt{\frac{k}{m}}. \tag{7}$$

For feedback control design, these parameters are estimated, such that the magnitude and the phase of (6) accord with those of the measured frequency responses as shown in Fig. 5. The estimated parameters are listed in Table II. Fig. 5 clearly shows that the model captures the first resonance at 54 Hz and 990 Hz of the Lorentz and piezo actuators, respectively. Since the delay is also captured well, the model shows a good fit at least up to 1.5 kHz. Above the frequency, parasitic dynamics can be seen for both actuators.

IV. ACTUATOR DEFINITION & MODEL-BASED ANALYSIS

After the influence of feedback control on the transmissibility is discussed, low-stiffness actuators are defined and analyzed to derive design rules to construct them in this section.

A. Transmissibility with feedback control

For the improvement of motion control performance, feedback control can be used to reject disturbances including vibrations [8] and to compensate for actuator non-linearity (e.g. creep or hysteresis) [20]. For discussion on the actuator categories, a feedback controller $C(s)$ is introduced as shown in Fig. 7, where r and e are position reference and error, respectively. Feedback control influences the transmissibility, and the transmissibility with feedback control can be derived by substituting $F(s)$ by $-G(s)C(s)K_sX_m(s)$ in (2) as follows

$$\frac{X_m(s)}{X_b(s)} = \frac{P_t(s)}{1 + P_a(s)G(s)C(s)K_s} = P_t(s)S(s), \tag{8}$$

Post-print version of the article: S. Ito and G. Schitter, "Comparison and Classification of High-Precision Actuators Based on Stiffness Influencing Vibration Isolation," *IEEE/ASME Transactions on Mechatronics*, vol. 21(2), pp. 1169-1178, 2016. DOI: 10.1109/TMECH.2015.2478658

This article has been accepted for publication in a future issue of this journal, but has not been fully edited. Content may change prior to final publication. Citation information: DOI 10.1109/TMECH.2015.2478658, IEEE/ASME Transactions on Mechatronics

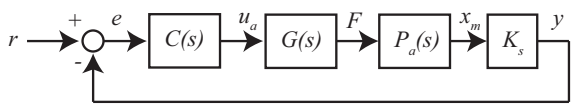

Fig. 7. Control block diagram of high-precision actuator and sensor $G(s)P_a(s)K_s$ with feedback control $C(s)$, where r and e are position reference and error, respectively.

where $S(s)$ is the sensitivity function of the feedback loop, which is equivalent to the transfer function from r to e. In order to eliminate a steady-state position error, typically $S(s)$ has high-pass characteristics with a low gain at low frequencies.

B. Actuator definition and analysis

An actuator with good vibration isolation must decouple the actuator position x_m from the vibrations x_b within a required frequency band. Furthermore, as the floor vibrations may contain shocks with low and high frequency components, it is desirable that the actuator does not amplify the vibrations transmitting to x_m at any frequencies for high-precision motion control. Since vibration transmission is quantized by the transmissibility, characterized by high vibration isolation (cf. Table I), a low-stiffness actuator is defined as the ones with a transmissibility that is less than 0 dB for all frequencies. Consequently, high-stiffness actuators are ones that are neither zero- nor low-stiffness. Therefore, high-stiffness actuators are defined as ones with a transmissibility that reaches or even exceeds 0 dB at some parts of the spectrum.

The definition of the low-stiffness actuators can be described by replacing s by $j\omega$ in (8) as

$$\left|\frac{X_m(j\omega)}{X_b(j\omega)}\right| = |P_t(j\omega)S(j\omega)| < 1, \quad \forall\omega. \tag{9}$$

The sensitivity function $S(j\omega)$ in positioning systems typically has a magnitude less than 0 dB at low frequencies to track the reference r. At high frequencies, the magnitude is larger than 0 dB due to the waterbed effect [7]. In-between $|S(j\omega)|$ crosses the 0 dB line at a frequency, which is defined as the unit-gain cross-over frequency of the sensitivity function ω_s (i.e. $|S(j\omega_s)| = 1$). Since $|S(j\omega)|$ can be 1 or larger for $\omega \geq \omega_s$, the magnitude of the transmissibility without control $|P_t(j\omega)|$ needs to be at least smaller than 1 in the frequency range to satisfy (9), as formulated in the following necessary condition

$$|P_t(j\omega)| < 1, \quad for \quad \omega \geq \omega_s. \tag{10}$$

For the passive vibration isolation behavior of $P_t(j\omega)$, its magnitude is less than one for all frequencies larger than $\sqrt{2}\omega_n$ as follows

$$|P_t(j\omega)| < 1, \quad for \quad \omega > \sqrt{2}\omega_n, \tag{11}$$

where ω_n is the undamped natural frequency. The frequency $\sqrt{2}\omega_n$ is derived by solving $|P_t(j\omega)| = 1$. From (11), the condition of (10) is satisfied only in the frequency range larger than $\sqrt{2}\omega_n$, resulting in the following requirement to design a low-stiffness actuator

$$\sqrt{2}\omega_n < \omega_s. \tag{12}$$

Since ω_n is given by $\sqrt{k/m}$, the above equation can be rewritten as

$$k < m\omega_s^2/2. \tag{13}$$

Although the discussion above holds with any damping coefficient c, it is typically far less than the critical damping for high-precision actuators (i.e. $\zeta \ll 1$). For vibration isolation, this characteristics is often favorable because a damper introduces dynamic coupling at high frequencies due to the zero in the transmissibility (4) [7]. With such a low damping coefficient, ω_n can be approximated by the resonant frequency ω_r, and the following design rule is also applicable in practice

$$\sqrt{2}\omega_r < \omega_s. \tag{14}$$

The left hand side of this equation is the lowest frequency of the passive vibration isolation. Similarly, the right can be regarded as the highest frequency of the disturbance rejection by the feedback control (i.e. active vibration isolation). Therefore, (14) can be interpreted that low-stiffness actuators are realized by a combination of active and passive vibration isolation in the frequency domain, as illustrated in Fig. 8(a). In other words, low-stiffness actuators achieve smooth transition from the active to the passive vibration isolation. In contrast, high-stiffness actuators can have a gap between the passive and active vibration isolation in the frequency domain as shown in Fig. 8(b). Thus, the vibrations from the base are even amplified on the moving part in a certain frequency band.

Required control bandwidth of actuators can also be discussed with (14). Since it is typically higher than ω_s [21], the control bandwidth of low-stiffness actuators has to be higher than the resonant frequency ω_r. This requirement implies that some feedback controllers are not suitable for low-stiffness actuators, particularly I, PI and PII controllers, because ω_r restricts the control bandwidth with these controllers for stability [18], [22]. In contrast, there is no requirement on the control bandwidth to construct high stiffness actuators, and it can be less than ω_r dependent on the control design.

Note that the discussion in this section is applicable to any feedback control described by $C(s)$, since its structure has not been specified. For the experiments in this paper, $C(s)$ is designed by using H_∞ control synthesis in the next section.

V. Control Design

For a fair comparison of the actuators presented in Section II, feedback controllers are individually designed, such that their cross-over frequency ω_s is about 350 Hz. With this frequency, the Lorentz and piezo actuators become low-stiffness and high-stiffness actuators, respectively according to (14) because of the difference in the first resonant frequency (cf. Fig. 5). Because the upper bound of the sensitivity function $S(s)$ can be shaped with proper weights, H_∞ control synthesis [21] is selected for the feedback control design.

A. H_∞ control synthesis

Fig. 9 shows a control block diagram with weighting functions for the control synthesis. Because its inverse is the

This article has been accepted for publication in a future issue of this journal, but has not been fully edited. Content may change prior to final publication. Citation information: DOI 10.1109/TMECH.2015.2478658, IEEE/ASME Transactions on Mechatronics

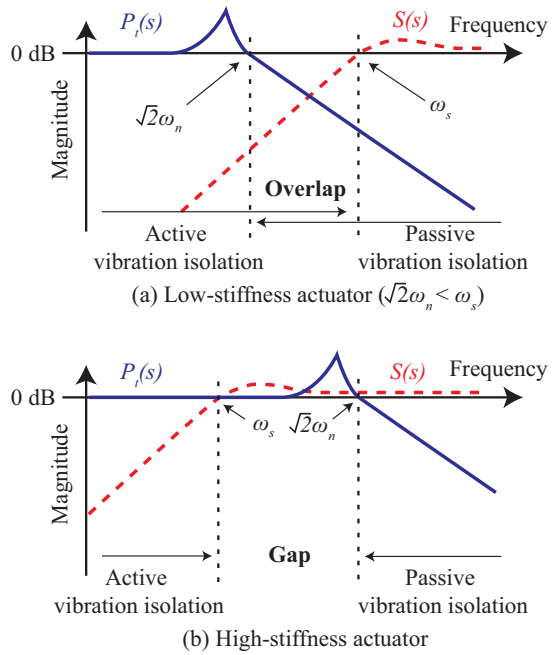

Fig. 8. Conceptual Bode plot of low-stiffness actuator (a) and high-stiffness actuator (b), showing sensitivity function $S(s)$ and transmissibility without feedback control $P_t(s)$. The unit-gain cross-over frequency of $S(s)$ is pointed by ω_s. Symbol ω_n is the natural frequency of the system.

upper bound of $S(s)$, the weight $W_s(s)$ on $S(s)$ has low-pass characteristics as follows

$$W_s(s) = 0.1\frac{s + 2\pi \cdot 2500}{s + 2\pi \cdot 0.2}. \tag{15}$$

Transfer function $W_t(s)$ is the weight on the complementary sensitivity function $T(s)$ (i.e. transfer function from r to y). This weighting function is given as follows

$$W_t(s) = 0.6\frac{s^2/\omega_{t1}^2 + 1.4s/\omega_{t1} + 1}{s^2/\omega_{t2}^2 + 1.4s/\omega_{t2} + 1}. \tag{16}$$

The parameter ω_{t1} and ω_{t2} are tuned, such that $S(s)$ crosses over the 0 dB line along the upper bound. Signal d is added between the controller and the plant model with its tuning parameter W_d, which prevents controller zeros from canceling the plant poles. The controller $C(s)$ is obtained by minimizing the H_∞ norm of the transfer function from r and d to the weighted signal z_s and z_t, that is

$$\left\| \begin{bmatrix} W_s(s)S(s) & -W_dW_s(s)G(s)P_a(s)K_sS(s) \\ W_t(s)T(s) & W_dW_t(s)G(s)P_a(s)K_sS(s) \end{bmatrix} \right\|_\infty. \tag{17}$$

Using the block diagram, three feedback controllers are designed. The controller $C_{P1}(s)$ is designed for the piezo actuator under $W_d = 0$, with which the plant poles are canceled by the controller zeros, similar to a notch filter. In the case of $C_{P2}(s)$ and $C_L(s)$ for the piezo and Lorentz actuators, respectively, W_d is not zero to prevent the pole-zero cancellation. With the non-zero setting, $C_{P2}(s)$ shifts the phase around the resonant frequency for stability (cf. [23]). Similarly, $C_L(s)$ provides phase lead at the open-loop cross-over frequency, as it is done by a PD controller or a phase-lead compensator [24]. The tuning parameter values used for the control design are listed in Table III.

TABLE III
TUNING PARAMETER VALUES FOR CONTROL DESIGN

Parameter	$C_{P1}(s)$	$C_{P2}(s)$	$C_L(s)$
Target actuator	Piezo		Lorentz
W_d	0	0.015	
ω_{t1}	$2\pi \cdot 500$	$2\pi \cdot 1000$	$2\pi \cdot 500$
ω_{t2}	$2\pi \cdot 3000$	$2\pi \cdot 5000$	$2\pi \cdot 3000$

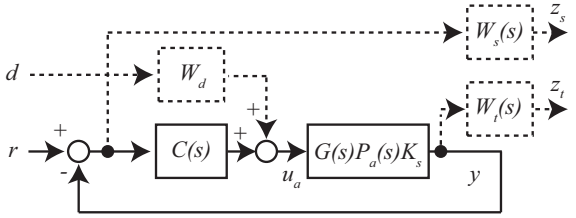

Fig. 9. Control block diagram used for feedback control design. Transfer function $G(s)P_a(s)K_s$ represents an actuator with its driver and the sensor, and $C(s)$ is the controller to be designed. The dashed-line blocks are weighting functions required for the control design.

B. Validation

For the validation of the control design and implementation, the sensitivity function $S(s)$ is measured as shown in Fig 10. In all the three cases, the crossing of the 0 dB line is seen at around 350 Hz, as intended in the design. In addition, the measured $S(s)$ with $C_{P2}(s)$ and $C_L(s)$ shows a notch at approximately 1 kHz and 50 Hz, respectively. This is because their first mechanical resonance increases the open-loop gain and contributes to the disturbance rejection. However, such a notch cannot be seen with $C_{P1}(s)$ since its zeros cancel the plant poles. Therefore, the mechanical resonances can be utilized for disturbance rejection under feedback control, which is not restricted by the actuator categories, but is dependent on the control design.

The complementary sensitivity function is shown in Fig. 11, where the -3 dB bandwidth is between 500 Hz and 700 Hz in all three cases. As discussed in Section IV, it is higher than the resonant frequency of the Lorentz actuator as a low-stiffness actuator (54 Hz), while it is lower than that of the piezo as a high-stiffness actuator (990 Hz).

C. Simulation

For further investigation of the control design, the transmissibility with control (8) is simulated based on the nominal model (4) and (6), as shown in Fig 12. The Lorentz actuator with $C_L(s)$ shows the transmissibility less than -19 dB for the entire frequency range, which satisfies the low-stiffness actuator definition (9), as desired. In the case of the piezo with

Post-print version of the article: S. Ito and G. Schitter, "Comparison and Classification of High-Precision Actuators Based on Stiffness Influencing Vibration Isolation," *IEEE/ASME Transactions on Mechatronics*, vol. 21(2), pp. 1169-1178, 2016. DOI: 10.1109/TMECH.2015.2478658

This article has been accepted for publication in a future issue of this journal, but has not been fully edited. Content may change prior to final publication. Citation information: DOI 10.1109/TMECH.2015.2478658, IEEE/ASME Transactions on Mechatronics

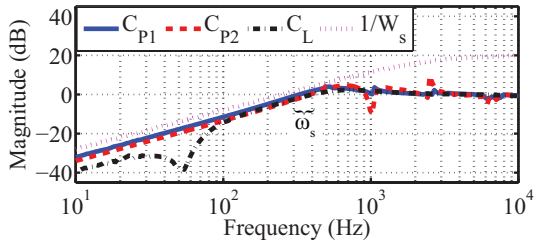

Fig. 10. Sensitivity function $S(s)$ measured for validation of control design and implementation with inverse of weighting function $W_s(s)$. Controller $C_{P1}(s)$ and $C_{P2}(s)$ are implemented for the piezo actuator, while $C_L(s)$ is for the Lorentz actuator. Symbol ω_s indicates the corresponding unit-gain cross-over frequencies.

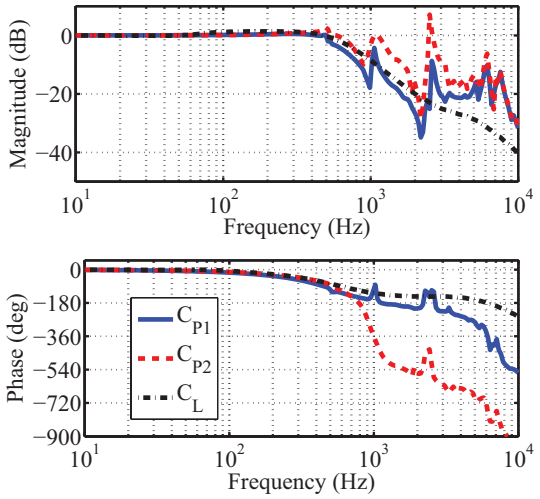

Fig. 11. Complementary sensitivity function $T(s)$ measured for validation of control design and implementation. Controller $C_{P1}(s)$ and $C_{P2}(s)$ are implemented for the piezo actuator, while $C_L(s)$ is for the Lorentz actuator.

$C_{P1}(s)$ and $C_{P2}(s)$, it behaves as a high-stiffness actuator, showing the transmissibility larger than 0 dB approximately between 300 Hz and 1.5 kHz.

For investigation in the time domain, response to a step in the actuator base position x_b is simulated, since steps contain high frequency components. The step height is set at 160 nm, which is almost the same stimulus as the experiments in Section VI. Fig 13(a)(b) shows the simulated actuator position x_m. The maximum value of x_m is 245 nm and 216 nm at approximately 0.4 ms for the piezo with $C_{P1}(s)$ and $C_{P2}(s)$, respectively, and particularly the response with $C_{P1}(s)$ shows a long lasting oscillation due to the excited mechanical resonance at about 1 kHz. In the case of the Lorentz actuator with $C_L(s)$, the maximum value of x_m is only 9.07 nm, demonstrating good vibration isolation of a low-stiffness actuator. For the step input, the control input u_a (i.e. reference to the actuator amplifier) is also simulated as shown in Fig 13(c)(d). For this simulation, a transfer function from

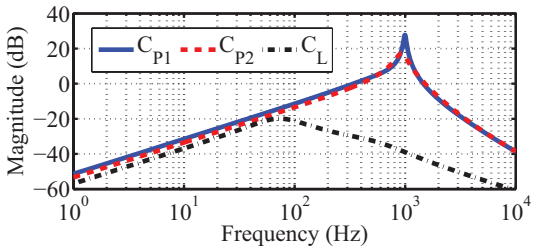

Fig. 12. Simulated transmissibility of bending piezo with designed feedback controller $C_{P1}(s)$ and $C_{P2}(s)$, as well as Lorentz actuator with $C_L(s)$.

x_b to u_a is derived from Fig. 7 and (2) as follows

$$\frac{U_a(s)}{X_b(s)} = -K_s C(s) P_t(s) S(s). \tag{18}$$

To compensate for the step of x_b, the simulated control input converges to a certain value, which is different for each actuator, due to the difference in the actuator gain g of Table II.

VI. Experiments

In order to validate the design rule, experiments in the frequency and time domain are presented. The measured data in this section is corrected with the sensor sensitivity K_s and the shaker sensitivity of 1621 nm/V as a part of the calibration. However, the shaker dynamics shown in Fig. 4 is not removed from the data, resembling an actual case how it may occur in a real system and demonstrating that the design rule (14) is applicable to practical high-precision mechatronic systems, where such unwanted parasitic dynamics are often inevitably occur.

A. Frequency response

The transmissibility of the actuators without feedback control is shown in Fig 14. The magnitude of the Lorentz actuator crosses the 0 dB line at 72 Hz, which is close to $\sqrt{2}\omega_n (\approx 76\,\text{Hz})$ as discussed with (11). In the case of the piezo, however, such clear trend cannot be seen due to the parasitic dynamics of the actuator and the shaker. Among the shaker resonances in Fig. 4, the largest at 500 Hz can be clearly observed with both actuators.

Fig. 15 shows the transmissibility of the actuators with the designed controllers, where the 2 kHz bandwidth limit due to the shaker determines the maximum frequency. The Lorentz actuator achieves the transmissibility of -40 dB at a low frequency of 10 Hz for good vibration isolation. While the experimental results show trends similar to the simulation in Fig. 12 at low frequencies, the magnitude in Fig. 15 increases at 546 Hz and 834 Hz due to the parasitic dynamics. Nevertheless, the Lorentz actuator achieves the transmissibility of less than -10 dB for the entire frequency range, satisfying the definition of the low-stiffness actuators (9). The trend change of the transmissibility at approximately 70 Hz is due to the smooth transition from the active to the passive vibration isolation, as discussed with Fig. 8(a).

This article has been accepted for publication in a future issue of this journal, but has not been fully edited. Content may change prior to final publication. Citation information: DOI 10.1109/TMECH.2015.2478658, IEEE/ASME Transactions on Mechatronics

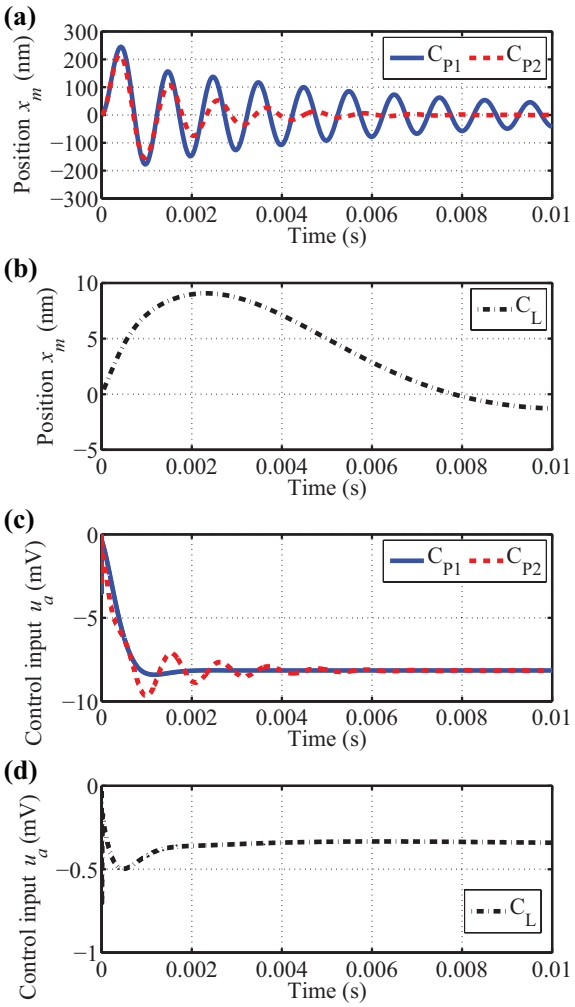

Fig. 13. Simulated response to a 160 nm step in actuator base position x_b: (a) position x_m of piezo actuator with $C_{P1}(s)$ and $C_{P2}(s)$, (b) position x_m of Lorentz actuator with $C_L(s)$, (c) control input u_a from $C_{P1}(s)$ and $C_{P2}(s)$, and (d) control input u_a from $C_L(s)$.

The bending piezo in Fig. 15 also shows good vibration isolation at a low frequency of 10 Hz, where the transmissibility is about -33 dB. However, it amplifies the vibrations due to the transmissibility larger than 0 dB approximately between 300 Hz and 1.6 kHz, because neither the active nor the passive vibration isolation is effective in the band (cf. Fig 8(b)). Although the controller $C_{P2}(s)$ trims the peak at the resonant frequency of 990 Hz, the magnitude still exceeds 0 dB.

B. Step response

As a demonstration in the time domain, since it contains high frequency components, a step of 100 mV, which corresponds to 162 nm, is given to the shaker amplifier to move the shaker in the direction of $-x_b$ (i.e. expanding the piezoelectric stack actuators). During the experiment, the feedback control is active to keep the respective actuator position x_m at a static position, and the position error e is recorded as shown in Fig. 16. The error of the bending piezo swings between ± 200 nm, because the step input excites the mechanical resonances, as it can also be seen in the power spectral density shown in Fig. 16(d). In the case of the Lorentz actuator, however, the error is suppressed within a range of ± 10 nm, since the vibration isolation is effective for the entire frequency range as a low-stiffness actuator (cf. Fig. 15). In comparison with the simulation in Fig. 13, Fig. 16(d) shows that the step input excites unmodeled dynamics, such as the shaker's resonance at 500 Hz. Nevertheless, Fig. 16(c) shows a small position error of the Lorentz actuator, demonstrating good vibration isolation as a low-stiffness actuator.

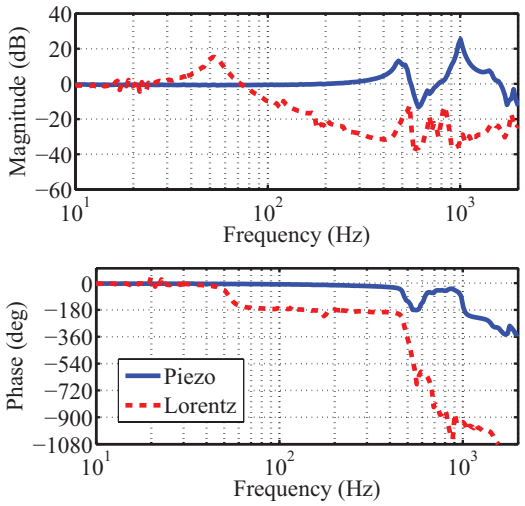

Fig. 14. Measured transmissibility of the bending piezo and the Lorentz actuator without feedback control.

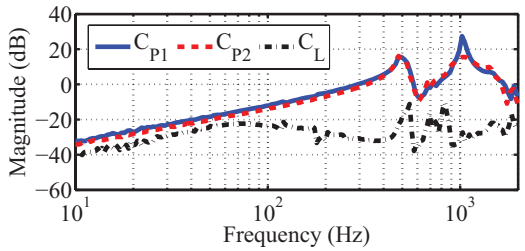

Fig. 15. Measured transmissibility of bending piezo with designed feedback controller $C_{P1}(s)$ and $C_{P2}(s)$, as well as Lorentz actuator with $C_L(s)$.

VII. Discussion

In Section IV low-stiffness actuators have been defined as ones that reject disturbances from the base for the entire frequency range, and high-stiffness actuators are neither zero- nor low-stiffness actuators. From the definition, the spring constant required to construct low-stiffness actuators have been derived in (13) as a design rule. Since its upper bound can be regarded

Post-print version of the article: S. Ito and G. Schitter, "Comparison and Classification of High-Precision Actuators Based on Stiffness Influencing Vibration Isolation," *IEEE/ASME Transactions on Mechatronics*, vol. 21(2), pp. 1169-1178, 2016. DOI: 10.1109/TMECH.2015.2478658

This article has been accepted for publication in a future issue of this journal, but has not been fully edited. Content may change prior to final publication. Citation information: DOI 10.1109/TMECH.2015.2478658, IEEE/ASME Transactions on Mechatronics

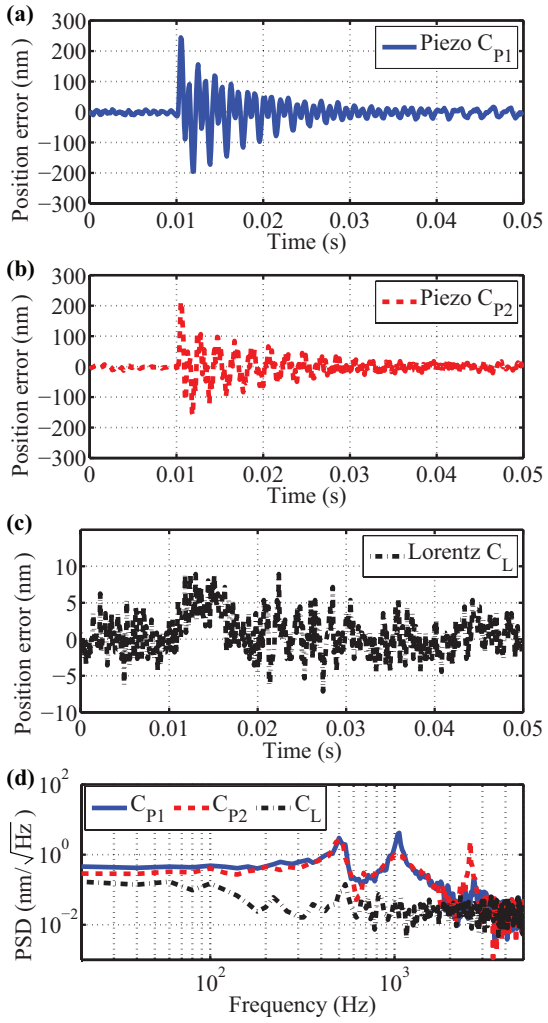

Fig. 16. Measured position error e during positioning at a static point. Step-like disturbances of approximately 160 nm are applied to the actuator base x_b at 0.01 s by using the shaker. Plot (a) and (b) show the response of the bending piezo controlled by $C_{P1}(s)$ and $C_{P2}(s)$, respectively, and (c) shows the response of the Lorentz actuator controlled by $C_L(s)$. The last plot (d) is the power spectral density of the position error.

as the border between low- and high- stiffness actuators, the spring constant is related to the actuator categories as shown in Table IV.

The stiffness requirement for low-stiffness actuators can be rephrased in the frequency domain as: "the cross-over frequency of the sensitivity function of the feedback-controlled system must be larger than the product of $\sqrt{2}$ and the resonant frequency ω_r of the uncontrolled system (cf. (14))". Whereas the resonant frequency ω_r can be a target value in the mechanical design (e.g. by using finite element analysis), the sensitivity function is utilized in the control design, specifying requirements on the electronics for control implementation as well as on power electronics for driving the actuator. Therefore, the design rule to construct low-stiffness actuators

TABLE IV
RELATION OF SPRING CONSTANT AND ACTUATOR CATEGORIES USING TRANSMISSIBILITY WITH FEEDBACK CONTROL $T_r(j\omega)$ AND CROSS-OVER FREQUENCY OF SENSITIVITY FUNCTION ω_s

Categories	Definition	Spring constant
Zero-stiffness	No mechanical connection	$k = 0$
Low-stiffness	$\lvert T_r(j\omega)\rvert < 1$ for all frequencies ω	$0 < k < m\omega_s^2/2$
High-stiffness	$\lvert T_r(j\omega)\rvert \geq 1$ at certain frequencies ω	$m\omega_s^2/2 \leq k$

can be regarded as a link between the mechanical design and the control design in the development of mechatronic systems. In each design phase sufficient margins need to be added to the design rule, since it is derived as a necessary condition.

Although the proposed design rule (14) does not specify the actuation principle of a low-stiffness actuator, satisfying it is difficult with piezos for vibration isolation in practice. This is typically because their first resonant frequency ω_r is too close to other resonant frequencies to ensure closed-loop stability for (14) (cf. Fig. 5). In contrast, the frequency band between the first and the other resonances of Lorentz actuators can be broad by design (cf. Fig. 5), making them more suitable to construct a low-stiffness actuator.

The proposed design rule (14) can be used in high-precision applications. An example is AFMs, where the probe is moved by a Lorentz or piezo actuator [2], [25]. For imaging, AFMs are typically mounted on an external vibration isolator, such as an optical table requiring an air compressor. By using a low-stiffness actuator satisfying (14) to move the probe, vibration isolation can be integrated in an AFM, instead of using a bulky external vibration isolator. Very first results of an AFM using low-stiffness actuators for vibration isolation can be found in [26]. In such a practical system, an application system (e.g. an AFM probe) is mounted as a part of the low-stiffness actuator's moving part. To prevent its internal modes from limiting the control bandwidth, the application system needs to be sufficiently rigid.

Unlike the ideal damped-mass-spring model used in the derivation of the rule, model uncertainty exits, such as the parasitic dynamics of the shaker. Nevertheless, as experimentally validated in Section VI, a precision actuator can be compact and have good vibration isolation properties for the entire frequency range by satisfying the proposed design rule.

VIII. CONCLUSION

This paper compares the vibration isolation properties of low-stiffness and high-stiffness actuated positioning systems. A Lorentz actuated and piezoelectrically actuated vibration isolation systems are compared by using the same control objectives for designing and implementing H_∞ feedback controllers for both systems. These systems are eventually experimentally validated. From the system analysis, a classification and design guidelines are derived for selecting the first resonance of the actuator (i.e. stiffness) and the corresponding disturbance-rejection bandwidth.

This article has been accepted for publication in a future issue of this journal, but has not been fully edited. Content may change prior to final publication. Citation information: DOI 10.1109/TMECH.2015.2478658, IEEE/ASME Transactions on Mechatronics

Low-stiffness actuators are defined as a closed-loop system with an actively controlled transmissibility less than 0 dB for the entire frequency range. Forming a clear border with high-stiffness actuators, the definition leads to a design rule of low-stiffness actuators that the cross-over frequency of the closed-loop sensitivity function must be larger than $\sqrt{2}$ times the first resonant frequency of the uncontrolled system. Under this condition, an actuator is able to achieve smooth transition from the active to the passive vibration isolation in the frequency domain. In contrast, systems with high-stiffness actuators, defined as neither zero- nor low-stiffness actuators, even amplify the vibrations in the gap between the active and passive vibration isolation.

REFERENCES

[1] H. Butler, "Position control in lithographic equipment," *IEEE Control Systems Magazine*, vol. 31, no. 5, pp. 28 –47, 2011.
[2] P. Eaton and P. West, *Atomic Force Microscopy*. Oxford University Press, 2010.
[3] T. Yamaguchi, M. Hirata, and C. Pang, *High-Speed Precision Motion Control*. Taylor & Francis, 2011.
[4] T. Atsumi and W. C. Messner, "Compensating for ZOH-induced residual vibrations in head-positioning control of hard disk drives," *IEEE/ASME Transactions on Mechatronics*, vol. 19, no. 1, pp. 258–268, 2014.
[5] J.-H. Lee and K.-J. Kim, "A method of transmissibility design for dual-chamber pneumatic vibration isolator," *Journal of Sound and Vibration*, vol. 323, no. 12, pp. 67 – 92, 2009.
[6] K.-S. Park, S. Lim, Y.-P. Park, Y.-B. Chang, and N.-C. Park, "Shock and vibration isolation of laptop hard disk drive using rubber mount," *Microsystem Technologies*, vol. 18, pp. 1559–1566, 2012.
[7] R. Munnig Schmidt, G. Schitter, A. Rankers, and J. van Eijk, *The Design of High Performance Mechatronics*, 2nd ed. Delft University Press, 2014.
[8] S. Ito, J. Steininger, and G. Schitter, "Low-stiffness dual stage actuator for long rage positioning with nanometer resolution (In press)," *Mechatronics*, 2015.
[9] Y.-M. Choi and D.-G. Gweon, "A high-precision dual-servo stage using halbach linear active magnetic bearings," *IEEE/ASME Transactions on Mechatronics*, vol. 16, no. 5, pp. 925–931, Oct 2011.
[10] B. Hou, J. Gao, and Y. Zhou, "The development of an ultra-precision dual-stage based on a master-slave control system," in *International Conference on Computer Distributed Control and Intelligent Environmental Monitoring*, March 2012, pp. 727 –730.
[11] M.-G. Song, Y.-K. Kim, N.-C. Park, J. Yoo, Y.-P. Park, N. Onagi, and G. Akanuma, "Design of moving magnet type pickup actuator using inserted coil," *Microsystem Technologies*, vol. 15, pp. 1719–1728, 2009.
[12] D.-J. Lee, M.-G. Song, C. Kim, N.-C. Park, Y.-P. Park, N. Onagi, and G. Akanuma, "Improvement of dynamic characteristics for symmetric-type slim optical pickup actuator by changing coil shape," *IEEE Transactions on Magnetics*, vol. 43, no. 2, pp. 808–810, Feb 2007.
[13] A. H. Chaghajerdi, "Sensing and control in optical drives," *IEEE Control Systems Magazine*, vol. 28, no. 3, pp. 23 –29, 2008.
[14] M. Heertjes and G. Leenknegt, "Switching control in blu-ray disk drives," *Mechatronics*, vol. 20, no. 4, pp. 453 – 463, 2010.
[15] Y. K. Yong, S. O. R. Moheimani, B. J. Kenton, and K. K. Leang, "Invited review article: High-speed flexure-guided nanopositioning: Mechanical design and control issues," *Review of Scientific Instruments*, vol. 83, no. 12, p. 121101, 2012.
[16] Y. K. Yong, B. Bhikkaji, and S. O. R. Moheimani, "Design, modeling, and FPAA-based control of a high-speed atomic force microscope nanopositioner," *IEEE/ASME Transactions on Mechatronics*, vol. 18, no. 3, pp. 1060–1071, June 2013.
[17] G. Schitter, K. J. Astrom, B. E. DeMartini, P. J. Thurner, K. L. Turner, and P. K. Hansma, "Design and modeling of a high-speed afm-scanner," *IEEE Transactions on Control Systems Technology*, vol. 15, no. 5, pp. 906 –915, 2007.
[18] A. J. Fleming, "Nanopositioning system with force feedback for high-performance tracking and vibration control," *IEEE/ASME Transactions on Mechatronics*, vol. 15, no. 3, pp. 433–447, June 2010.
[19] G. Schitter, P. J. Thurner, and P. K. Hansma, "Design and input-shaping control of a novel scanner for high-speed atomic force microscopy," *Mechatronics*, vol. 18, no. 56, pp. 282 – 288, 2008.
[20] Y. Shan, J. E. Speich, and K. K. Leang, "Low-cost IR reflective sensors for submicrolevel position measurement and control," *IEEE/ASME Transactions on Mechatronics*, vol. 13, no. 6, pp. 700–709, 2008.
[21] S. Skogestad and I. Postlethwaite, *Multivariable Feedback Control*. John Wiley, 2005.
[22] D. Y. Abramovitch, S. B. Andersson, L. Y. Pao, and G. Schitter, "A tutorial on the mechanisms, dynamics, and control of atomic force microscopes," in *American Control Conference*, July 2007, pp. 3488–3502.
[23] M. Kobayashi, S. Nakagawa, and S. Nakamura, "A phase-stabilized servo controller for dual-stage actuators in hard disk drives," *IEEE Transactions on Magnetics*, vol. 39, no. 2, pp. 844–850, Mar 2003.
[24] W. C. Messner, M. D. Bedillion, L. Xia, and D. C. Karns, "Lead and lag compensators with complex poles and zeros," *IEEE Control Systems Magazine*, vol. 27, no. 1, pp. 44–54, Feb 2007.
[25] H. Barnard, C. Randall, D. Bridges, and P. K. Hansma, "The long range voice coil atomic force microscope," *Review of Scientific Instruments*, vol. 83, no. 2, pp. –, 2012.
[26] S. Ito, D. Neyer, S. Pirker, J. Steininger, and G. Schitter, "Atomic force microscopy using voice coil actuators for vibration isolation," in *IEEE/ASME International Conference on Advanced Intelligent Mechatronics*, July 2015, pp. 470–475.

Shingo Ito received his M.A.Sc. degree in mechanical and industrial engineering from the University of Toronto, ON, Canada, in 2007. From 2007 to 2010, he worked as an engineer in the field of motion control at Yaskawa Electric Corporation, Iruma, Japan.

Currently he works toward his Ph.D. degree at the Automation and Control Institute (ACIN), the Vienna University of Technology, Austria. His research interest includes design and control of mechatronic systems and high-precision motion control.

Georg Schitter (SM'11) is Professor at the Automation and Control Institute (ACIN) of the Vienna University of Technology. He received an MSc. in Electrical Engineering from TU Graz, Austria (2000) and his PhD degree from ETH Zurich, Switzerland (2004).

His primary research interests are on high-performance mechatronic systems and multidisciplinary systems integration, particularly for precision engineering applications in the high-tech industry, scientific instrumentation, and mechatronic imaging systems, such as scanning probe microscopy, adaptive optics, and lithography systems for semiconductor industry.

He serves as Associate Editor for the IEEE/ASME Transactions on Mechatronics (2010-2014) as well as for the IFAC Journals Control Engineering Practice and IFAC Mechatronics.

Post-print version of the article: S. Ito and G. Schitter, "Comparison and Classification of High-Precision Actuators Based on Stiffness Influencing Vibration Isolation," *IEEE/ASME Transactions on Mechatronics*, vol. 21(2), pp. 1169-1178, 2016. DOI: 10.1109/TMECH.2015.2478658